Transactions, SMiRT-24
BEXCO, Busan, Korea - August 20-25, 2017
Division V, Paper 406

NEW ASCE 4 STANDARD-BASED PROBABILISTIC SOIL-STRUCTURE INTERACTION (SSI) ANALYSIS FOR SEISMIC DESIGN-BASIS ANALYSIS AND FRAGILITY CALCULATIONS

Dan M. Ghiocel[1]

[1] Chief of Engineering and President, Ghiocel Predictive Technologies, Inc., New York, USA

INTRODUCTION

Probabilistic soil-structure interaction (SSI) analysis is capable of capturing in much more detail the uncertainties related to the seismic motion, soil layering and structural behaviour than deterministic SSI analysis. In the introduction of the new ASCE 04-2016 standard (2017) it is stated that the purpose of the analytical methods included in the standard is to provide reasonable levels of conservatism to account for seismic analysis uncertainties. More specifically, in the same section it is written that given the seismic design response spectra input, the goal of the standard is that based on a set of recommendations to develop seismic deterministic SSI responses which correspond approximately to the 80% non-exceedance probability level (NEP). Thus, for seismic SSI analyses, the probabilistic responses defined with the 80% NEP are considered adequate. The paper illustrates the application of the new ASCE 04-16 standard recommendations for probabilistic SSI analysis applicable to both the design-basis level (DBE) applications and the beyond design-basis level (BDBE) applications including fragility analyses. The ACS SASSI software (2016) with Options PRO and NON is used for this paper.

PROBABILISTIC MODELING PER ASCE 4-16 STANDARD

The ASCE 4-16 standard Section 5.5 (ASCE, 2017) recommends for probabilistic SSI analysis the application of stochastic simulation using the Latin Hypercube Sampling (LHS). The ASCE 4-16 standard addresses both the probabilistic site response analysis (PSRA) and the probabilistic SSI analyses (PSSIA) in Sections 2 and 5.5, respectively.

Probabilistic modelling should usually include the random variations due to:

- Response spectral shape model for the seismic input
- Low-strain soil shear wave velocity Vs and hysteretic damping D profiles for each soil layer
- Soil layer shear modulus G and hysteretic damping D as random functions of soil shear strain
- Equivalent linear/effective stiffness and damping for concrete structural elements depending on stress/strain levels in different parts of the structure

The ACS SASSI Option PRO modules include the above probabilistic modelling aspects following the ASCE 4-16 standard recommendations for both PSRA and PSSIA (Ghiocel, 2015). Figure 1 shows a generic chart of the Option PRO PSSIA simulations.

For the probabilistic SSI response simulations, the input is represented as an ensemble of randomized seismic input motion sets. Each set consists of two horizontal components and one vertical component. The seismic motion spectral amplitude is assumed to be a lognormally distributed random variable or vector/field. Option PRO includes two probabilistic simulation methods for generating input acceleration time histories that are recommended in the ASCE 04-2016 standard Section 5.5 (Figure 2):

1) Method 1 that assumes that spectral shape is deterministic, constant shape curve, and
2) Method 2 that assumes that spectral shape is a random, variable shape curve.

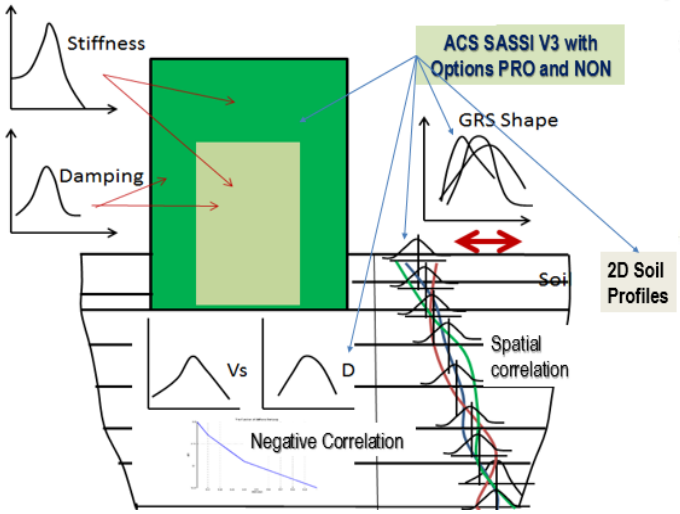

Figure 1 Probabilistic Seismic SSI Analysis Chart

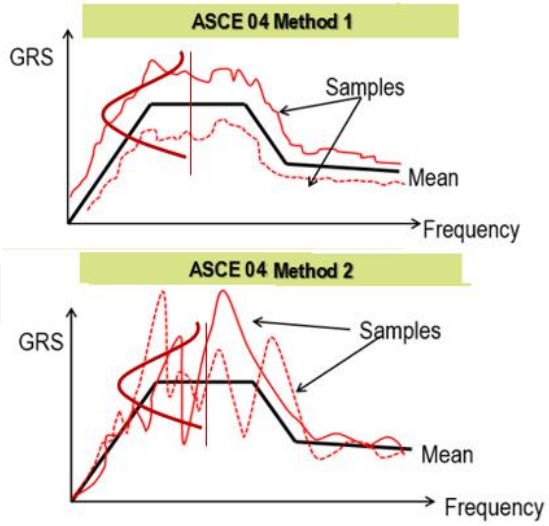

Figure 2 Probabilistic Seismic GRS Models

The low-strain Vs and D per soil layers are assumed to be statistically dependent lognormal or normal random variables. The statistical dependence is due to their joint dependence on the soil shear strain in each layer. In Option PRO, there are several options implemented to address the Vs and D statistical dependence. Each geological layer including several computational soil layers can be defined with different statistics, as means, coefficients of variation and correlation lengths. Thus, in general, the soil profiles are made of several segments for which the soil profile spatial correlation with depth is assumed to be constant. The soil profile simulations are based on the probability transformed-space Karhunen-Loeve expansion models (Figure 3).

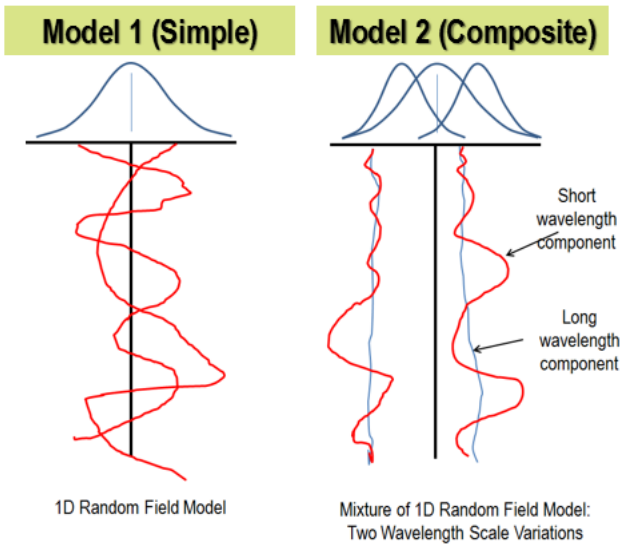

Figure 3 Probabilistic Soil Property Profile Models

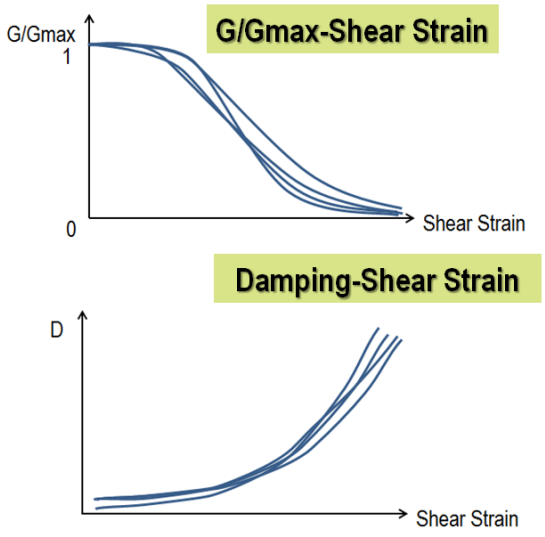

Figure 4 Probabilistic Soil Material Curves

The soil Vs and D profiles are assumed to be either i) Model 1, 1D random field with a spatial correlation structure with depth, or ii) Model 2, a random field mixture of a short-wavelength 1D component and a large-wavelength 1D component. The first modelling option produces ergodic field samples, while the second modelling option produces non-ergodic field samples since it contains two sources of

uncertainties. The Model 2 was also recommended by the Princeton university researchers based on various soil field measurements (Popescu, 1996). The selection of the soil profile model should be made based on the Vs field measurements on the site. The soil shear modulus G and damping D curves as functions of the soil shear strain in each layer, are modelled as 1D random field models with slow-variations or large wavelength in the shear strain space (Figure 4).

For structural modelling, the effective stiffness and damping values in the concrete walls should be defined as separated random variables for different parts of the structure which have different local stress/strain levels. Defining the effective stiffness and damping for each wall could be a labour intensive activity since for each seismic simulation, the stress/strain levels in the structure may vary substantially. The ACS SASSI Option NON can be used to automatically compute the effective stiffness and damping in the concrete walls as function of the local shear or bending strain.

The ACS SASSI Option PRO includes a number of seven probabilistic modules that generate the LHS randomized samples for the PSSIA input. These probabilistic modules include the ProEQUAKE, ProSOIL, ProSITE, ProHOUSE, ProMOTION, ProSTRESS and ProRESPONSE modules. A probabilistic analysis, either PSRA or PSSIA, there are three distinct steps to be completed: 1) Generate an ensemble of simulated probabilistic input files using LHS with the Option PRO pre-processing modules, 2) Run the ensemble of LHS sample input files to compute the corresponding SSI response files with the ACS SASSI main software modules, and 3) Post-process statistically the ensemble of the LHS responses with the Option PRO post-processing modules.

DESIGN-BASIS LEVEL (DBE) CASE STUDY

Probabilistic and deterministic SSI analyses were comparatively performed for a deeply embedded SMR SSI model. The probabilistic SSI analyses assumed that the spectral shape of the site-specific ground response spectra, the soil stiffness and damping profiles were idealized as random fields. The structural stiffness and damping random variations were modelled as a pair of correlated random variables that depend on the computed structural stress levels. The comparative SSI results include in-structure response spectra (ISRS) at different locations. The probabilistic SSI analysis results for the mean ISRS and 84% NEP ISRS (slightly higher than the 80% NEP ISRS) are compared with the deterministic SSI analysis envelope ISRS computed including the three deterministic soil profile variations, namely, lower bound (LB), best-estimate (BE) and upper bond (UB).

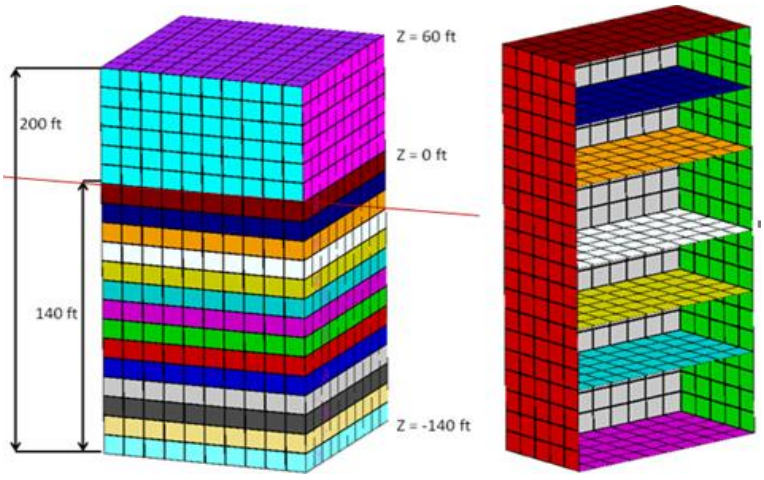

Figure 5 140 ft Embedded SMR SSI Model

Figure 5 shows the deeply embedded SMR SSI model. The SMR structure has a size of 200ft x 100ft x 100ft (H x L x W) with an embedment of 140ft depth (Ghiocel, 2014). The soil profile shown in Figure 6 is highly non-uniform with a soil layer stiffness variation inversion within the embedment depth. The seismic motion was input at the SMR foundation level (FIRS) at the 140 ft depth (elevation 0 ft).

For probabilistic analyses, the in-column FIRS input motion were computed based on the probabilistic site response analysis using 60 LHS samples. The 60 randomized soil profiles are plotted in Figure 6. For statistical segments were considered for soil profile modelling. Both the Model 1 and the Model 2 were comparatively used for the soil profile probabilistic modelling. The statistics of the Vs and D soil profiles have variation coefficients of 20% and 30%, respectively. The Vs and D statistical dependence as function of soil shear strain level is captured by a coefficient of correlation of -0.40. The smoothness of the soil variation profiles was controlled by the correlation length parameters that vary with depth (for the four segments). The correlation lengths were considered 40 ft for the segments 1 and 3 down from the ground surface and 100 ft for the segments 2 and 4. These correlation length values were used for both the Model 1 and the Model 2 short-wavelength component variations. As shown in Figure 6, the probabilistic seismic input was defined by the outcrop UHRS motion simulated at the 500 ft depth bedrock.

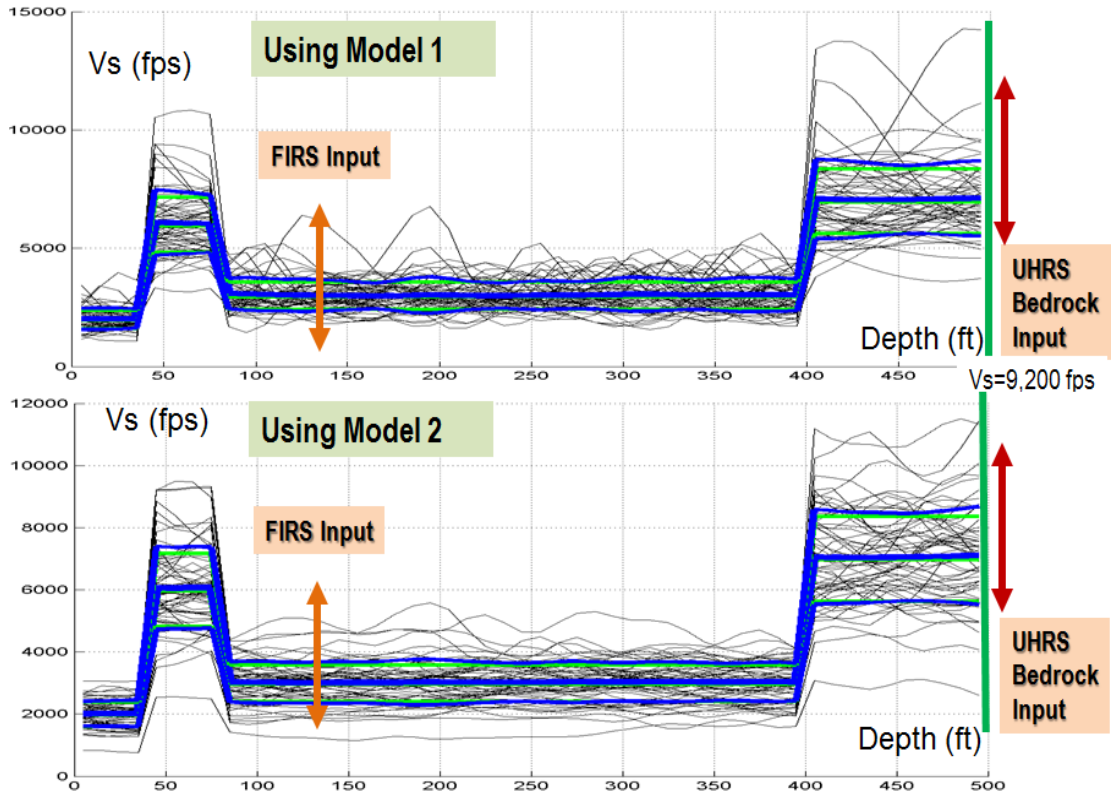

Figure 6 Vs Soil Profile Simulations; Random Samples (black), Simulated Statistical Curves (blue) Versus Target Statistical Curves (green)

The 60 simulations of the in-column FIRS obtained using PSRA are shown in Figure 7. The simulated in-column FIRS motions were further used for the PSSIA of the SMR structure. It should be noted that the two soil profile models, Model 1 and Model 2 (Figure 6), produce slightly different FIRS shapes for the random samples and the mean curves.

Probabilistic SSI ISRS results are shown in Figures 8 through 10. Each figure includes comparative ISRS probabilistic 84% NEP ISRS vs. deterministic ISRS for the two profile models, Model 1 and Model 2.

It should be noted that the deterministic seismic inputs are defined by the in-column FIRS computed for the LB, BE and UB soils based on the (probabilistic) mean outcrop UHRS FIRS obtained for the 60 probabilistic site response simulations. Thus, the deterministic SSI analysis is not based on the DRS FIRS input that is used in the "conventional" deterministic design-basis seismic analysis, that is a combination of the UHRS FIRS computed for two annual seismic hazard probabilities, namely, 1.e-4 and 1.e-5, as described in the ASCE 43-05 standard and its new ASCE 43-17 draft.

It should be noted that in general, the comparison of probabilistic and "conventional" deterministic SSI analysis results depends on the seismic hazard level considered for the probabilistic simulations. If the 1.e-4 annual seismic hazard probability is considered, then, the deterministic SSI results should go up by the ratio DRS/1.e-4 UHRS, while if the 1.e-5 annual seismic hazard probability is considered, the deterministic SSI results should go down by the ratio 1.e-5 UHRS/DRS. To avoid any confusion, the deterministic seismic input was defined by the same (probabilistic) mean UHRS/FIRS computed from probabilistic simulations, and not by the DRS/FIRS.

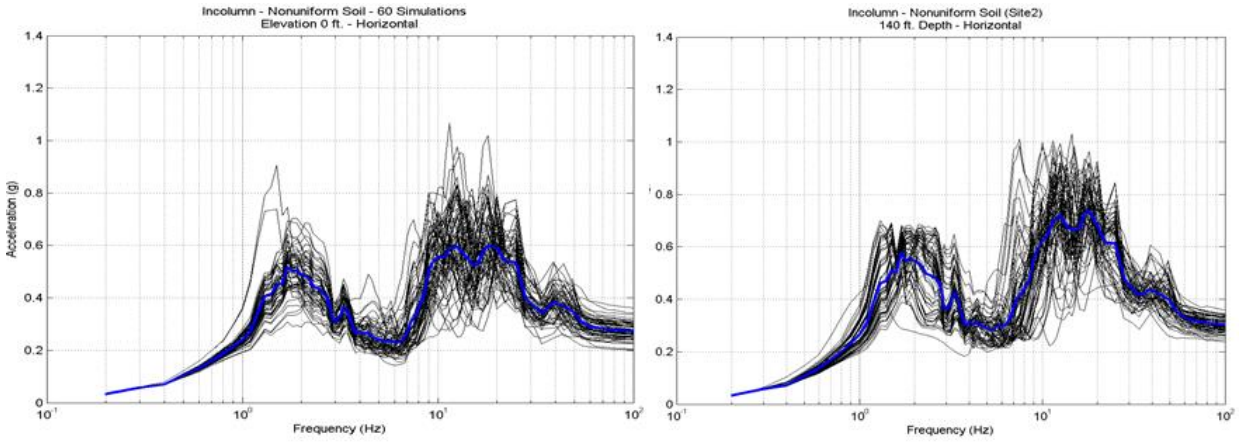

Figure 7 Simulated FIRS Using Model 1 (left) and Model 2 (right); Samples (black) and Mean (blue)

For probabilistic structural modeling, it was considered that the entire SMR model has the same effective stiffness and damping modeled as lognormal random variables. The effective stiffness was assumed with a mean of 0.80 times the elastic stiffness and a c.o.v of 10%, while the effective damping was assumed with a mean of 6% and a c.o.v. of 30%. The statistical dependence between the two variables was included by a negative correlation coefficient of -0.80. For deterministic structure modeling the uncracked stiffness and 4% damping were assumed.

Figures 8 thru 10 show comparisons of the deterministic ISRS for the LB, BE and UB soils, (red lines, with solid line for BE soil) and the probabilistic mean and 84% NEP ISRS (green lines, solid line for mean values) at 0ft elevation (basemat level) and 170ft elevation (30ft above ground level). The left side plots of the Figures 8 through 10 show the ISRS results based on the Model 1 soil profile (Figure 6, upper plot), while the right side plots show results based on the Model 2 soil profile (Figure 6, lower plot). It should be noted that the probabilistic model used for the simulation of the soil profiles affects slightly both the probabilistic and the deterministic ISRS. The deterministic soil profiles of Vs and D correspond to the 16%, mean, and 84% NEP statistical estimates, and, therefore, they are affected by the probabilistic soil profile modelling using Model 1 or Model 2.

Figures 8 and 9 show the ISRS computed at 0ft elevation (basemat) for the horizontal direction and vertical direction, respectively. The blue arrows on the plots indicate frequency bands for which some discrepancy between the probabilistic 84% NEP ISRS and the deterministic envelope ISRS are noticed. For the horizontal direction, as shown in Figure 8, at lower frequencies the probabilistic 84% NEP ISRS are slightly larger, up to 20% for Model 2, while in the high-frequency range, above 10 Hz, the deterministic ISRS, especially for the UB soil, has a much larger peak amplitude than the probabilistic 84% NEP ISRS, possibly with a 100% increase or even more. For the vertical direction, as shown in Figure 9, similar trends are noticed.

Figure 8 ISRS plots also indicate that the deterministic soil profiles, LB, BE and UB, produce a highly amplified SSI analysis responses in the 20-30 Hz range, since these profiles are basically outside of the range soil profile random variations. This is due the fact that producing a randomized soil profile that is similar to the deterministic soil profiles for which all soil layers are being simultaneously stiffer or softer, has a very low likelihood, or in other words, the deterministic soil profile corresponds to a small occurrence probability within the random sample space. In deterministic SSI analysis, the soil profiles have an implicit occurrence probability of unity since it corresponds to a sure event.

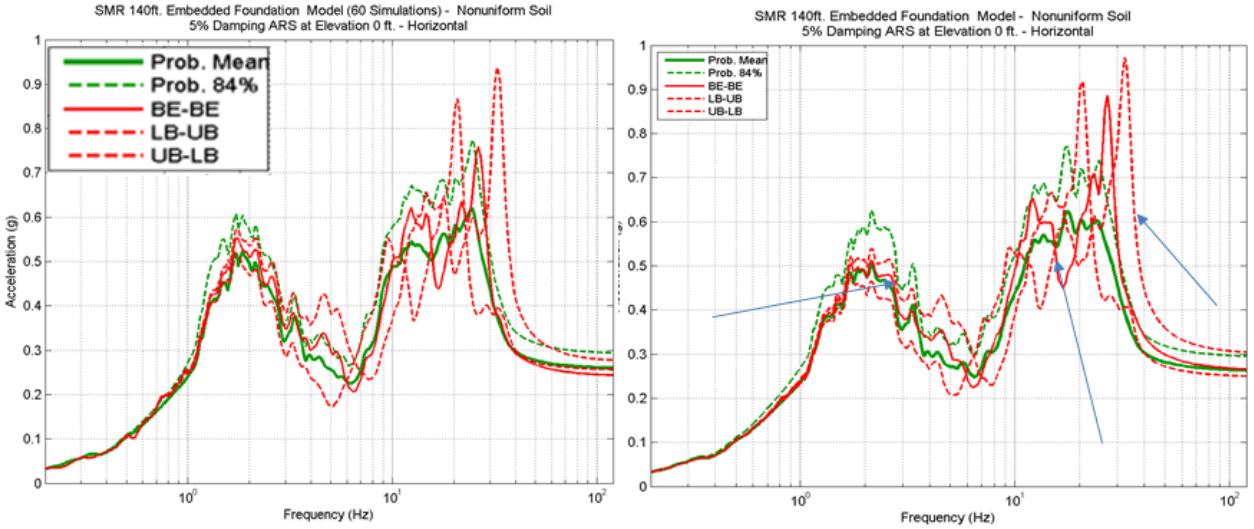

Figure 8 Horizontal ISRS at the Basemat Level Using Model 1 (left) and Model 2 (right) for Soil Profiles

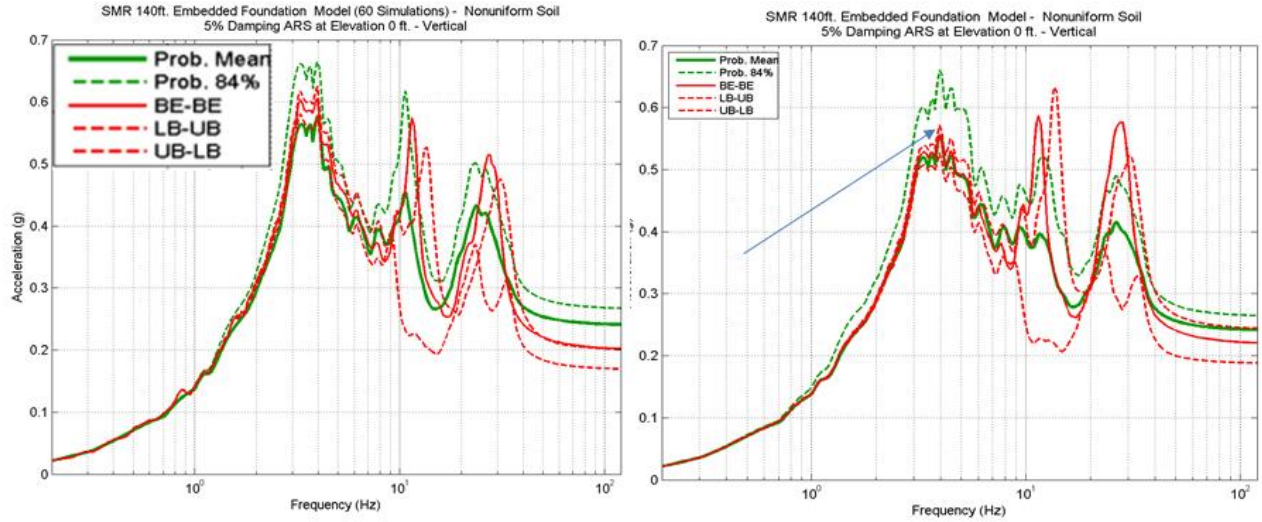

Figure 9 Vertical ISRS at the Basemat Level Using Model 1 (left) and Model 2 (right) for Soil Profiles

Figure 10 shows the horizontal ISRS computed at 170ft elevation (30ft above ground level). The deterministic envelope ISRS spectral peak, in fact only for the UB soil, is much larger than the probabilistic 84% NEP ISRS, about 50% larger. This significant difference between the deterministic and probabilistic ISRS is mainly due to the 4% low damping value used for the deterministic SSI analysis for the uncracked concrete that is lower than the randomized damping values assumed with a statistical mean of 6% for the probabilistic SSI analysis. It should be also noted that the deterministic envelope ISRS peak is at 7 Hz, while the probabilistic 84% NEP ISRS peak is at 5.5 Hz that is about 20% lower than the deterministic envelope ISRS peak. Also, the LB soil ISRS peak occurs at a frequency of 4.3 Hz, the BE soil ISRS peak occurs at 5.5 Hz, and the UB soil ISRS peak occurs at 7.0 Hz. The peak frequency shifts is about +/- 20% around the BE soil ISRS peak frequency. This 20% frequency shift raises the question if the traditional 15% ISRS broadening recommended in the ASCE standards is sufficient for the deeply SMR applications.

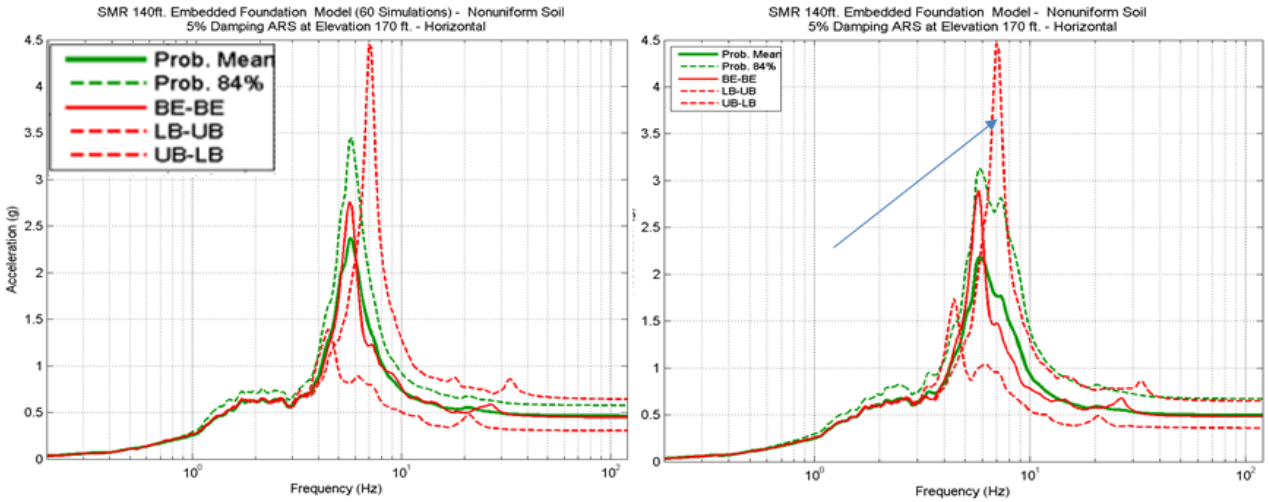

Figure 10 Horizontal ISRS at 30ft Above Ground Level Using Model 1 (left) and Model 2 (right)

The large horizontal deterministic ISRS peaks noticed in Figures 8 and 10 could appear to be a penalty of the deterministic SSI analysis on the economical aspects of the nuclear design. There is a urgent need for having more comparative probabilistic-deterministic investigations based on the ASCE 4-16 standard recommendations for various case studies.

BEYOND DESIGN-BASIS LEVEL (BDBE) CASE STUDIES

ASCE 4-16 Standard-Based Probabilistic SSI Analysis for Seismic Fragility and Risk Computations

Probabilistic SSI analyses for the beyond design-basis (BDBE) applications are typically performed for seismic input review levels that are much larger than the design-basis (DBE) seismic input, often by 2-3 times. For such much larger BDBE seismic inputs, the role of the nonlinear soil and structure behaviours become very important SSI modelling aspects for obtaining meaningful seismic margin results. Herein, the application of the probabilistic SSI analysis per the new ASCE 4-16 standard is presented in the context of the seismic fragility analyses.

The new ASCE 4-16 standard provides a probabilistic physics-based modelling framework for computing seismic SSI response variations that is a good basis for adequately deriving the fragility analysis data, and by this to substantially reduce the “expert” subjectivity. The “expert” subjectivity”, in many situations, can introduce significant, artificial biases in the SSC seismic margin evaluations which can be sometimes too crude, or even inappropriate on a case-by-case basis.

An accurate seismic fragility analysis should include several seismic hazard levels or review levels, not only a single seismic hazard level or review level. At the least, three seismic hazard levels or review levels should be considered as acceptable. For performing a pertinent probabilistic SSI analysis per the new ASCE 4-16 recommendations, probabilistic models for the seismic input motion, the soil profile and the structure should be defined for each seismic hazard level, as briefly described below:

- Probabilistic outcrop UHRS SEISMIC input at the bedrock should be defined for each review level. Usually, at the least three levels, 1e-4, 1e-5 and 1e-6 should be considered for the seismic hazard annual probability. Based the PSHA studies, the deaggregated bedrock UHRS inputs should be defined for the governing seismic events as functions of the magnitude and epicenter distance. Probabilistic models should assume that the bedrock UHRS frequency content has random variations.

- Probabilistic SOIL layer profiles should be defined for each review level are necessary. Probabilistic models should include at the least the shear velocity Vs, and damping D soil profiles and the material constitutive curves applicable for the soil condition sites. For the soil sites, the nonlinear soil behavior should be included for each review level and each seismic input simulation.

- Probabilistic STRUCTURE material properties, namely, the effective stiffness and damping, should be defined for each review level. Probabilistic models should include the effective stiffness and damping variations. Since the effective/equivalent-linear stiffness and damping properties are functions of the stress/strain level, their values are different for different parts of the structure. The nonlinear structure behavior should be included for each review level and each seismic input simulation.

The seismic hazard curve considered for the investigated case study that is for a rock site is shown in Figure 11. The maximum ground acceleration levels vary from 0.10g to 1.60g. The DBE level corresponds to the outcrop UHRS defined for a 0.25g maximum ground acceleration in the horizontal direction. The seismic hazard curve is used to define seven seismic hazard or review levels which correspond to the annual mean occurrence probabilities of 3.2.e-4, 1.0e-4, 3.2e-5, 1.0e-5, 3.2e-6, 1.0e-6 and 3.2e-7. The c.o.v. values associated to the seismic hazard curve are plotted by the yellow-brown line and vary from 50% at 0.10g to 100% at 1.60g.

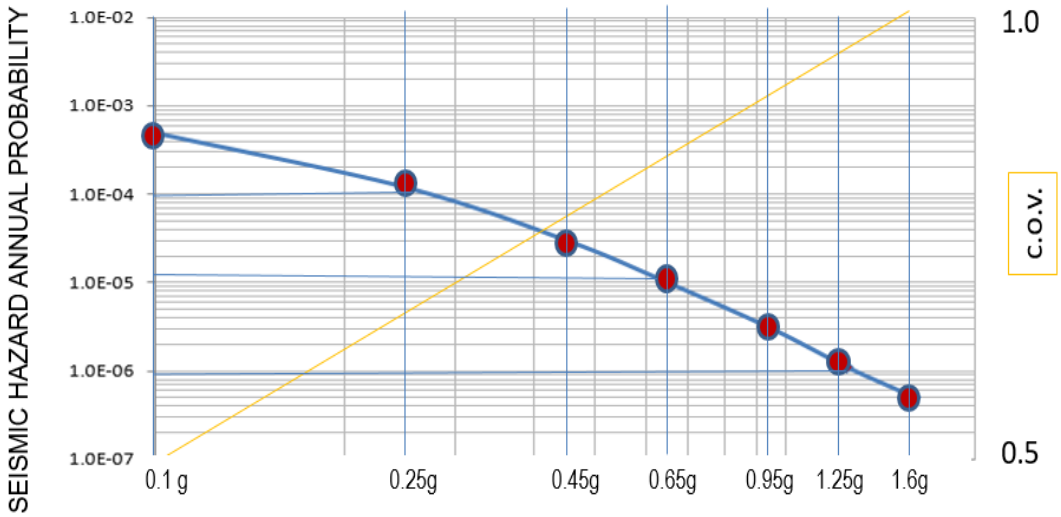

Figure 11 Seismic Hazard Curve for Investigated Rock Site

To compute the total seismic risk or failure probability curves for SSCs, the seismic hazard curve slope should be "convolved" with the SSC fragility curves as illustrated in Figure 12. The overall predicted risk including all seismic hazard events is finally obtained by integrating the total risk curve over the entire ground acceleration axis. It should be noted that the seismic hazard and fragility curves are affected by the epistemic or modelling uncertainties. These uncertainties are illustrated in Figure 12 by the probability density functions (blue colour areas) and their random samples (black lines). These uncertainties are further propagating to the total risk curves and, finally, to the overall predicted risk, Pf, affecting its confidence interval. The overall predicted risk should be determined with high confidence levels, since usually the overall risk estimate has large uncertain variations.

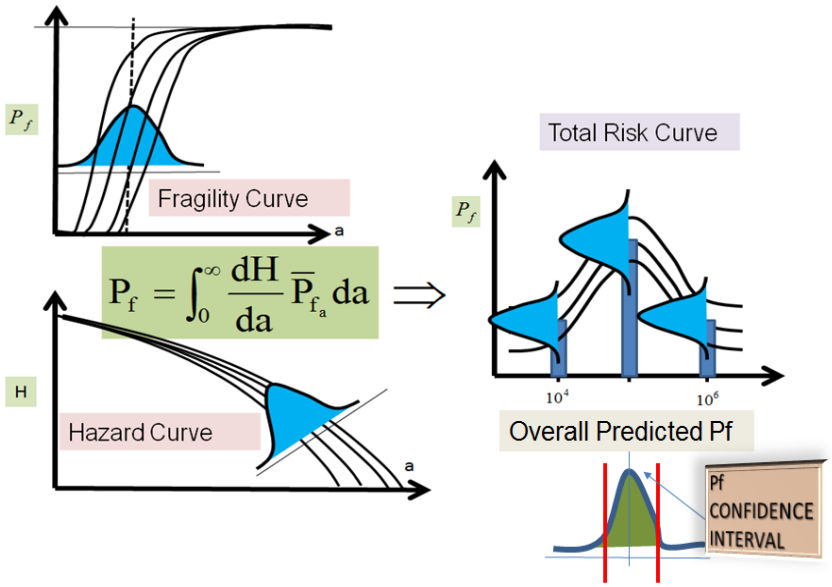

Figure 12 Total Seismic Risk Prediction Chart

The epistemic or modeling uncertainties were computed using the probabilistic seismic response variations for two sets of probabilistic SSI analysis, as follows:

1) Probabilistic SSI analysis including total or composite probabilistic variations composed by the superposition of the randomness variations and the epistemic or modeling uncertainty variations;

2) Probabilistic SSI analysis including only the random variations (with no epistemic uncertainties).

The epistemic or modeling uncertainty variations can be computed by subtracting the random variations from the total or composite variations of the seismic responses. The simulation procedure permits an accurate evaluation of the epistemic uncertainty variations based on computing the epistemic uncertainty variates for each pair of the 60 probabilistic response simulations produced in steps 1) and 2).

The probabilistic SSI analysis was performed for each of the seven selected seismic hazard or review levels using the ACS SASSI Option PRO software (2016). Figure 13 shows the 60 probabilistic outcrop UHRS input simulations which were used for the PSRA and the PSSIA computations for the 0.25g (design-basis) seismic hazard level input.

For each UHRS simulation, a spectrum compatible acceleration time history was generated. Since the investigated site is a rock site, the nonlinear soil behavior effects are negligible. For random variations, the UHRS amplitude was assumed to be a lognormal random variable with the mean equal to mean UHRS and a c.o.v. of 28%. The ASCE 4-16 Section 5.5 Method 2 with randomized UHRS spectral

shapes was applied (ProEQUAKE module). The correlation length was taken 10 Hz. To include the epistemic uncertainties a lognormal random factor with mean of 1.0 and c.o.v. of 25% was applied.

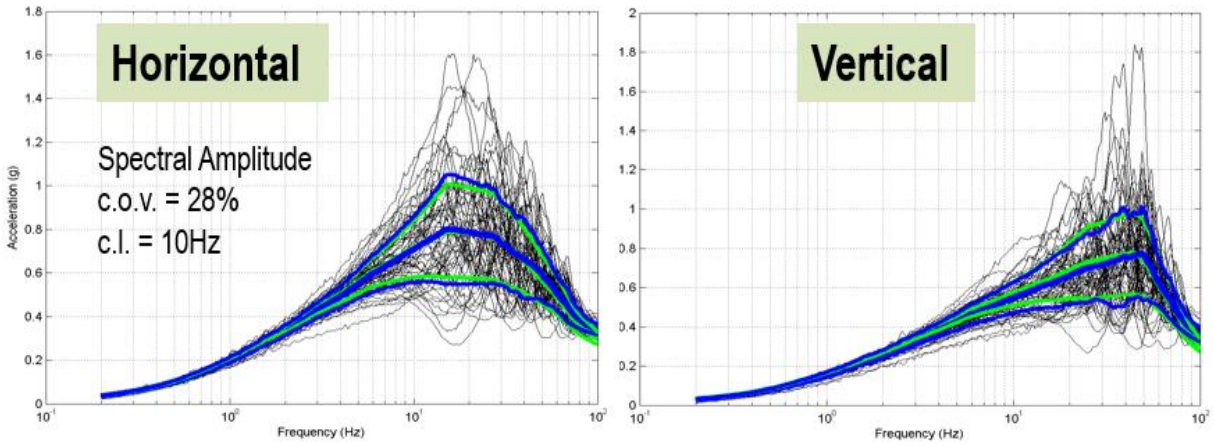

Figure 13 Probabilistic Horizontal and Vertical UHRS Simulations for 0.25g Seismic Input Level

The 60 probabilistic soil layering simulations are shown in Figure 14. For the randomness variations, the soil profile probabilistic modelling was based on the Model 2 that includes a mixture of two lognormal random field components, with a short wavelength and a long wavelength, respectively. The c.o.v. of the Vs and D soil profiles were 20%, with a c.o.v. of 14% for the short wavelength component and a c.o.v. of 15% for the long wavelength component. The correlation length were 100 ft for short wavelength component and 1000 ft for long wavelength component.

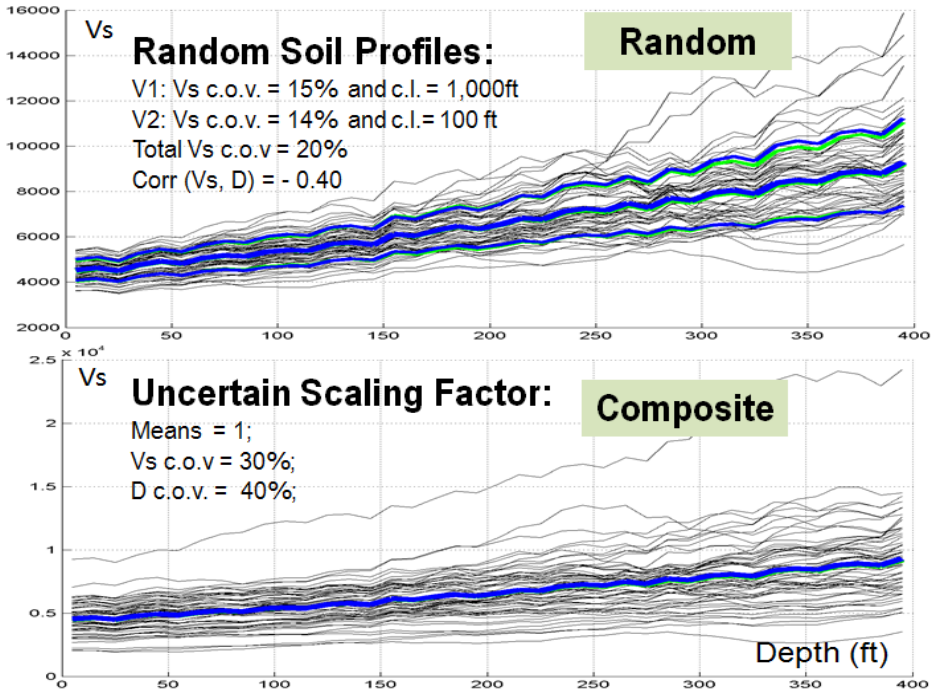

Figure 14 Vs Soil Profile Simulations for Random and Composite Variations

The statistical dependence between Vs and D was simulated by a correlation coefficient of -0.40. For the epistemic uncertainty variations of Vs and D profiles, lognormal random scale factors with a mean of 1.0 and c.o.v. of 30% and 40%, respectively, were considered.

The investigated concrete shearwall nuclear building used for probabilistic SSI analysis is shown in Figure 15. For the seismic inputs associated with seismic hazard levels which are well beyond the 0.25g design-basis level, up to 1.60g, the nonlinear structure behaviour is an important aspect of the SSI modelling. For the probabilistic nonlinear SSI analysis, the ACS SASSI Options NON and PRO modules were combined.

To include the nonlinear concrete behaviour, the structure model has to be split in a number of wall "panels". The wall panel is part of the concrete shearwall that is under a relative uniform shear or bending deformation. Herein, the investigated nuclear building nonlinear model included 40 wall panels, as shown in Figure 15 (Ghiocel, 2015, Ghiocel and Saremi, 2017).

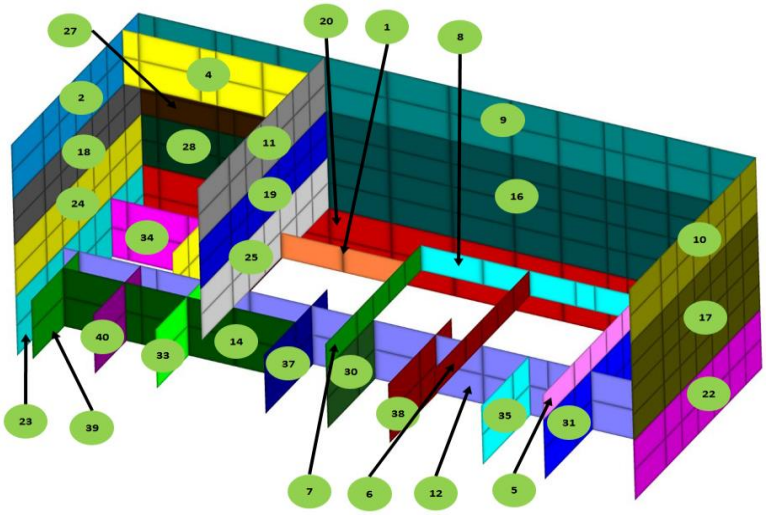

Figure 15 Low-Rise Reinforced Concrete Shearwall Building Nonlinear Model With 40 Wall Panels (the Basemat, Roof and Longitudinal External Wall are Removed)

For each nonlinear wall panel, a back-bone curve (BBC) has to be defined. The BBC curves should have a smooth shape and variation that describes the nonlinear behaviour of the wall panels under the lateral seismic loading. The smoothed BBC were automatically generated based on the input data on the cracking and ultimate capacity shear force values and assuming that the secant cracked stiffness between the cracking and yielding points is half of the uncracked stiffness as recommended in the ASCE 4-16 (Ghiocel and Saremi, 2017).

Figure 16 shows the 60 probabilistic simulations of the BBC for a given wall panel. The BBC were assumed to vary randomly assuming a lognormal random factor with mean of 1.0 and the c.o.v. of 15% for random variations and a c.o.v. of 33.5% for composite variations.

For the nonlinear hysteretic behaviour the Cheng-Mertz shear (CMS) hysteretic model was used (Ghiocel, 2015). This CMS hysteretic model is a part of the ACS SASSI Option NON library of hysteretic models. Figure 17 shows the CMS hysteretic shear force-shear strain loops for two different wall panels.

The shear strain capacities of the wall panels were assumed to have lognormal probability distributions with the mean of 0.5% and c.o.v. of 35% for random variations and c.o.v. of 45% for composite variations, respectively. The lognormal reliability model used to compute the wall shear failure probabilities (or fragilities) is described in Figure 18.

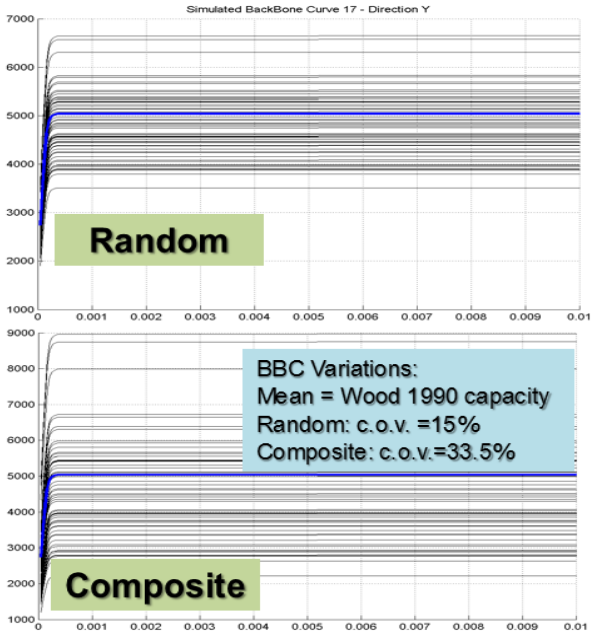

Figure 16 Back-Bone Curve (BBC) Simulations

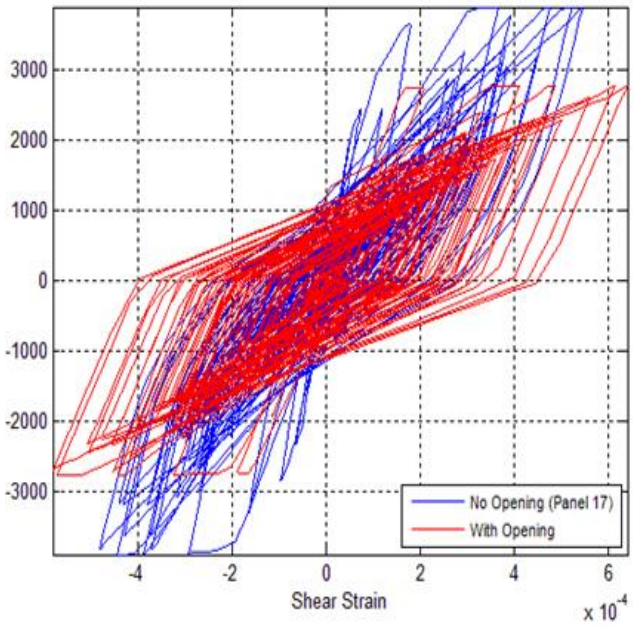

Figure 17 Cheng-Mertz Shear Hysteretic Loops

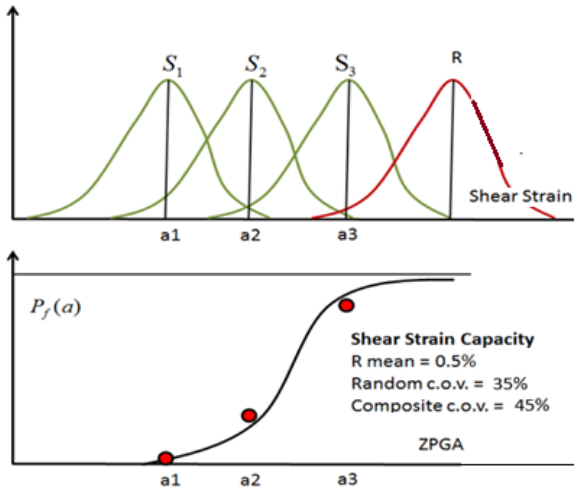

Figure 18 Shear Wall Failure Reliability Model

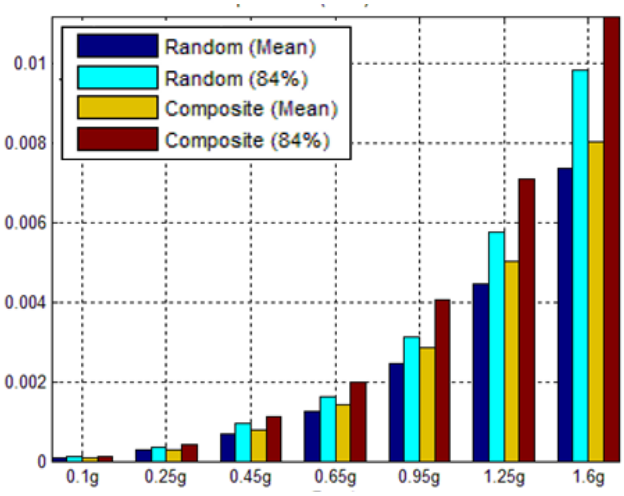

Figure 19 Wall Shear Strain Statistical Responses

Figures 19 through 22 shows the results obtained for the structural fragility analysis based on the physics-based probabilistic nonlinear SSI response simulations using the combined ACS SASSI Options PRO and NON software modules. Figure 19 shows the mean and 84% NEP shear strains computed in the transverse wall Panel 17 (see Figure 15 for panel locations) based on the random variations and the composite variations, respectively. All seven seismic review levels are included in Figure 19.

Figure 20 shows the hysteretic behaviour of Panel 17 for the 0.95g seismic hazard level for the random and composite variations, respectively, for the largest (blue) and smallest (red) story drift simulations.

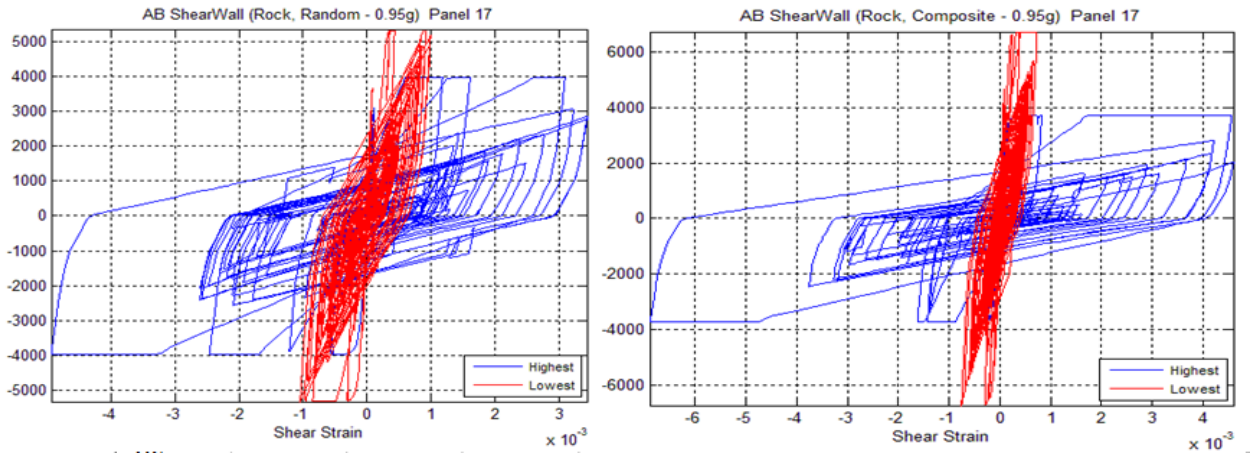

Figure 20 CMS Hysteretic Loops for 0.95g Review Level for Largest (blue) and Smallest (red) Simulated Responses; For Random Variations (left plot) and For Composite Variations (right plot)

Table 1 shows the epistemic uncertainty variations (U) computed based the two separate physics-based probabilistic nonlinear SSI analysis results obtained for the random variations (R) only, and the total or composite variations (C) including both random and epistemic uncertainty variations, respectively. The epistemic uncertainty variations for each response quantity of interest was computed for each probabilistic simulation j by Uj = Cj/Rj, as defined in the lognormal fragility format, where Cj is the simulated response including the composite variations and Rj is the simulated response including only the random variations. Then, based on the Uj responses for all the 60 simulations, j=1,60, the statistics of the U variable, the Umean and U c.o.v. were computed for each response quantity of interest. This procedure is based on the fact that the SEED numbers used for the probabilistic simulations of the random variations are the same in the two separate probabilistic SSI analyses.

Table 1 shows the U variable for the wall shear strain responses in the top seven panels which indicated the largest story drift responses. It should be noted that some U variables have a trend to shift upward from the mean of 1.0 for some responses and also increase their variations for larger seismic hazard levels. These trends are the largest for the transverse Panel 25 that behaves highly nonlinear behavior for larger seismic hazard levels. These trends also indicate the deviation of the physics-based computed U variable from the assumed lognormal format for the U variable.

Figure 21 shows the probabilistic 84% NEP story drift responses in all 40 wall panels (see Figure 15 for panel locations) for two seismic hazard levels, namely, the 0.10g and 1.25g. It should be noted that for the 0.10g level, the structure behaves linear elastically, and the story drift distribution across different walls is much more uniform than for the 1.25g level for which some walls behave heavily nonlinear and a result of this, the story drift distribution is highly non-uniform, in pockets of damages in few walls.

Table 1 Computed U Variable Statistics for Selected Wall Panel Story Drifts

Panel	0.25g		0.45g		0.65g		0.95g		1.25g		1.6g	
	U mean	U C.O.V.	U mean	U C.O.V.	U mean	U C.O.V.	U mean	U C.O.V.	U mean	U C.O.V.	U mean	U C.O.V.
15	1.0243	0.2585	1.0193	0.2328	1.0338	0.2255	1.0450	0.2286	1.0776	0.2612	1.0665	0.2559
16	1.0575	0.2526	1.0605	0.2816	1.1542	0.3697	1.2183	0.3494	1.2433	0.2982	1.2301	0.2545
17	1.0516	0.1719	1.0792	0.1884	1.0988	0.1964	1.0876	0.2320	1.0864	0.2525	1.0734	0.2683
24	1.0386	0.2621	1.1108	0.2664	1.2602	0.2841	1.2946	0.3333	1.2345	0.3240	1.1885	0.3482
25	1.0504	0.2346	1.1293	0.2968	1.1644	0.3078	1.1546	0.2924	1.1799	0.3709	1.2225	0.4778
28	1.0223	0.1492	1.0555	0.1934	1.0345	0.1515	1.0470	0.1660	1.0573	0.1802	1.0329	0.1936
29	1.0136	0.1467	1.0240	0.1763	1.0321	0.1667	1.0300	0.1700	1.0502	0.1678	1.0218	0.1866

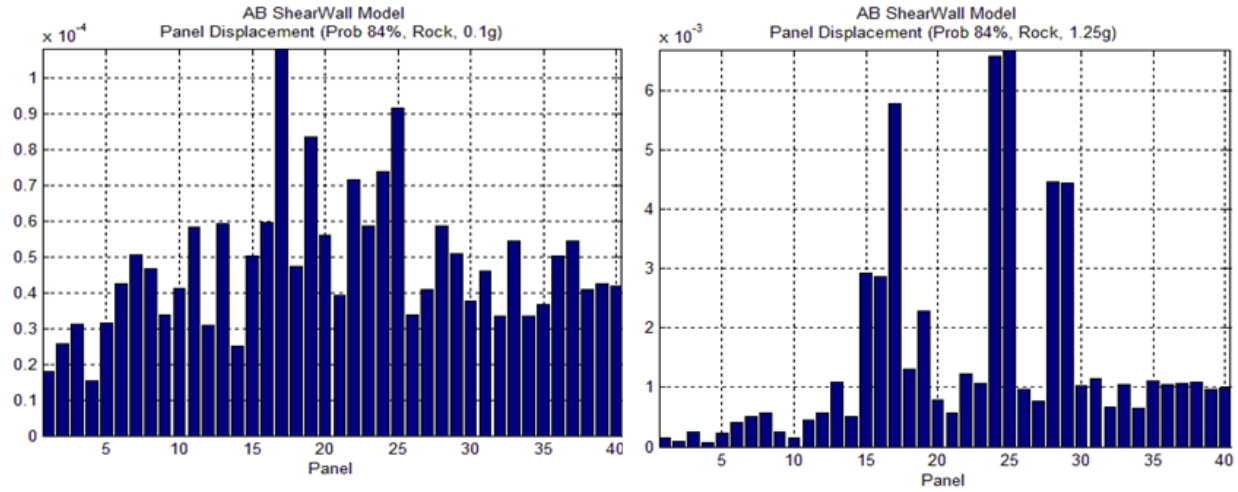

Figure 21 Probabilistic 84% NEP Story Drifts in Wall Panels for
0.10g (left) and 1.25g (right) Seismic Hazard Levels

For the 1.25g level, the story drifts are the largest in the panels 17, 24 and 25 in the transverse direction, and panels 28 and 29 in the longitudinal direction. The Figure 21 results show that the use of nonlinear SSI analysis is very important to capture more realistically the dynamic behaviour the building structure for large seismic input levels.

To compute the structural fragility curves for the concrete walls, the traditional lognormal format was applied. Based on the simulated probabilistic SSI responses and the probabilistic wall capacities, the conditional failure probabilities (fragility data points) were computed for all seven hazard levels using the lognormal reliability model. Then, a probability space transformation to normal space is applied to the computed probability data, and based on the linear regression in the normal space, the lognormal fragility curves were determined, as illustrated in Figure 22. The red colour corresponds to the composite fragility curve, while the blue colour corresponds to the mean fragility curve (no epistemic uncertainty included).

Finally the total risks and the overall risks were computed based on the panel structural fragility curves and the seismic hazard curve both assumed to follow the lognormal distribution format, as shown in Figure 12. To compute the total risks and the overall risk, a Monte Carlo simulation with 100,000 random samples was employed.

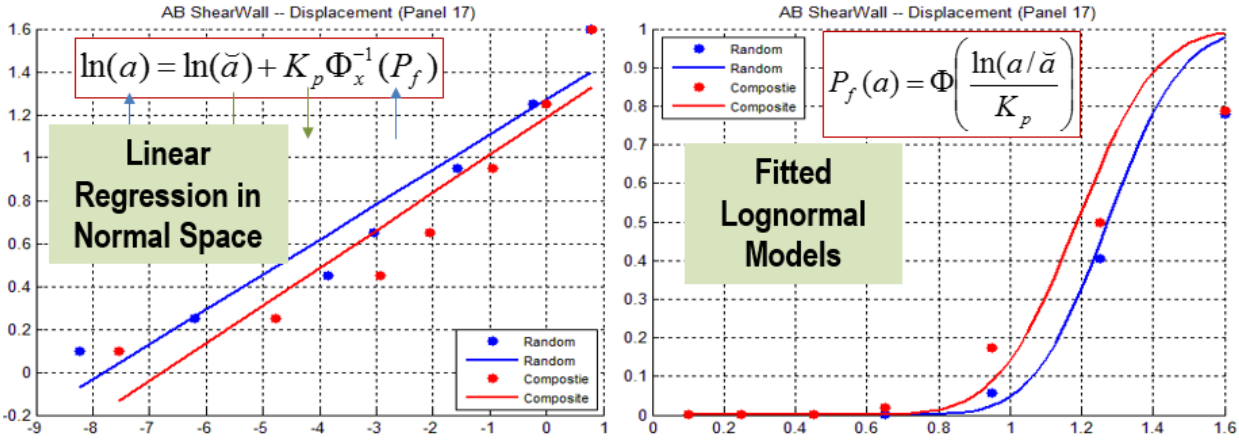

Figure 22 Fitted Lognormal Structural Fragility Curve vs. Computed Fragility Data for the Panel 17 Shear Failure Mode; Linear Regression in Normal Space (left) and Fitted Lognormal Fragility Curve (right)

Based on the probabilistic nonlinear SSI analysis simulations, the overall risks, Pf, were obtained for the following four scenarios:

i) Multipoint estimate approach using seven seismic hazard levels with annual probability of 3.2.e-4, 1.0e-4, 3.2e-5, 1.0e-5, 3.2e-6, 1.0e-6 and 3.2e-7
ii) Multipoint estimate approach using three seismic hazard levels with annual probability of 1.0e-4, 1.0e-5 and 1.0e-6,
iii) Point estimate approach using a single seismic hazard level with annual probability of 1.0e-4
iv) Point estimate approach using a single seismic hazard level with annual probability of 1.0e-5

Table 2 Overall Risk Pf Estimates for Four Seismic Hazard Level Scenarios
(Seven Levels, Three Levels and Two Single Levels)

Displacement Panel #	pf mean	pf C.O.V.	pf 90%CDF	pf 90%LOGN	pf 95%CDF	pf 95%LOGN	
15	1.82E-007	0.71	3.60E-007	3.38E-007	4.27E-007	4.27E-007	
16	2.40E-007	1.06	5.48E-007	5.02E-007	7.17E-007	6.88E-007	
17	7.80E-007	0.49	1.26E-006	1.27E-006	1.48E-006	1.50E-006	**7 ZPGA Levels**
24	8.78E-007	0.60	1.55E-006	1.53E-006	1.85E-006	1.87E-006	
25	9.22E-007	0.68	1.71E-006	1.68E-006	2.11E-006	2.10E-006	
28	4.59E-007	0.24	6.04E-007	6.04E-007	6.53E-007	6.58E-007	
29	4.16E-007	0.46	6.65E-007	6.65E-007	7.72E-007	7.81E-007	
Displacement Panel #	Random pf mean	pf C.O.V.	pf 90%CDF	pf 90%LOGN	pf 95%CDF	pf 95%LOGN	
15	3.94E-008	0.54	6.85E-008	6.63E-008	7.61E-008	7.96E-008	
16	4.34E-008	0.81	8.95E-008	8.39E-008	1.10E-007	1.09E-007	
17	6.67E-007	1.06	1.52E-006	1.39E-006	1.97E-006	1.91E-006	**3 ZPGA Levels**
24	6.56E-007	0.80	1.35E-006	1.26E-006	1.64E-006	1.63E-006	
25	6.17E-007	0.70	1.18E-006	1.13E-006	1.43E-006	1.42E-006	
28	2.98E-007	0.96	6.65E-007	6.06E-007	8.61E-007	8.13E-007	
29	2.30E-007	0.87	4.87E-007	4.54E-007	6.09E-007	5.96E-007	
Displacement Panel #	Random pf mean	pf C.O.V.	pf 90%CDF	pf 90%LOGN	pf 95%CDF	pf 95%LOGN	
15	5.20E-006	2.79	1.39E-005	1.16E-005	2.77E-005	1.98E-005	**1 ZPGA Level; 1e-4 or 0.25g**
16	1.51E-005	4.66	2.72E-005	3.13E-005	6.61E-005	5.85E-005	
17	4.39E-008	1.17	1.03E-007	9.38E-008	1.38E-007	1.32E-007	
24	8.14E-008	3.34	2.14E-007	1.79E-007	3.88E-007	3.17E-007	
25	3.26E-008	2.66	8.74E-008	7.34E-008	1.52E-007	1.24E-007	
28	2.61E-005	3.96	4.82E-005	5.54E-005	1.25E-004	1.01E-004	
29	4.49E-007	4.33	8.83E-007	9.40E-007	2.00E-006	1.74E-006	
Displacement Panel #	Random pf mean	pf C.O.V.	pf 90%CDF	pf 90%LOGN	pf 95%CDF	pf 95%LOGN	
15	1.41E-008	0.95	3.21E-008	2.85E-008	4.08E-008	3.81E-008	**1 ZPGA Level; 1e-5 or 0.65g**
16	2.47E-008	1.35	6.05E-008	5.43E-008	8.45E-008	7.85E-008	
17	3.48E-007	1.11	7.90E-007	7.34E-007	1.06E-006	1.02E-006	
24	2.46E-007	1.10	5.68E-007	5.18E-007	7.52E-007	7.17E-007	
25	2.22E-007	1.02	4.87E-007	4.59E-007	6.50E-007	6.23E-007	
28	7.78E-008	1.02	1.71E-007	1.61E-007	2.31E-007	2.18E-007	
29	4.98E-008	0.94	1.06E-007	1.00E-007	1.38E-007	1.34E-007	

Table 2 provides a comparison of the seismic overall risks, Pf, computed for the seven most affected wall panels. The predicted risk Pf are shown for three confidence levels, namely, the mean estimate, the 90% confidence estimate and the 95% confidence estimate.

The Table 2 results show large differences between the overall structural risks computed for the four seismic hazard scenarios. The multiple level/multipoint estimate approach provides significantly different risk predictions than the traditional one level/point estimate approach with SSI response scaling. Using 1.e-5 probability level with nonlinear SSI analysis as review level is better than using the 1.-e4 probability level with linear SSI analysis.

Further, the overall risks for the nuclear equipment systems were investigated based on the probabilistic SSI simulations performed for each seismic hazard level. The probabilistic seismic load for the equipment

systems is described by the probabilistic in-structure response spectra (ISRS) computed at the equipment system supports. The ISRS amplitude is assumed to have a lognormal probability distribution.

Figure 23 shows the probabilistic mean and 84% NEP ISRS for two locations, on the 4th floor at node 9 (higher elevation) and on the 2nd floor at node 576 (lower elevation).

The equipment capacity is assumed to be a lognormal variable with the minimum capacity defined for the 1% NEP that is taken equal to the 84% NEP ISRS for the 1.e-4 seismic hazard level of 0.25g that is assumed to be design-basis level.

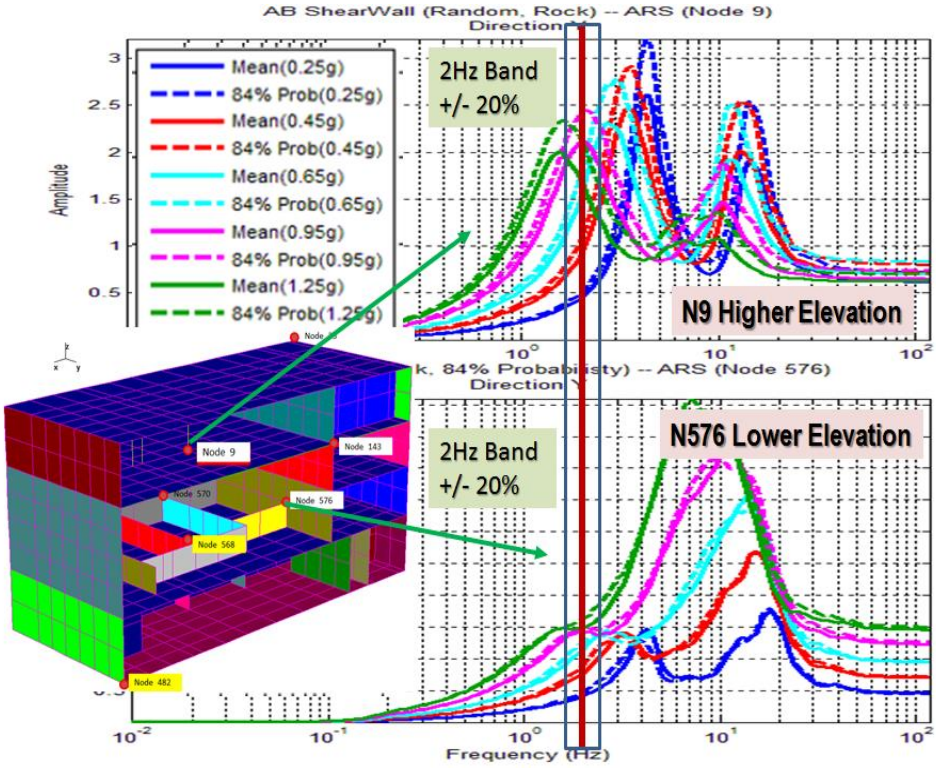

Figure 23 Probabilistic Mean and 84% NEP ISRS at Node 9 (4th Floor) and Node 576 (2nd Floor) Computed for Five Seismic Hazard Levels (not including the extremes 0.10g and 1.60g)

Figure 23 includes a +/- 20% band for a 2 Hz resonant frequency equipment at the two ISRS locations. The +/-20% frequency band is due to the equipment resonant frequency uncertainty. It should be noted that for the Node 9 ISRS the maximum spectral amplitude in the 2 Hz +/- 20% frequency band is not a monotonic function of the maximum ground acceleration due to the nonlinear structure behaviour for large seismic motions.

Figure 24 shows the fitted lognormal and the probability data-point fragility curves for the 2 Hz frequency equipment at the two locations, Node 9 and Node 576. It should be noted that the lognormal fragility curves deviates significantly from the probability data points computed for each seismic hazard level. As shown in Figure 24 upper plots, the Node 9 2Hz equipment fragility curve should have a non-monotonic variation with ground acceleration that is beyond the modelling capability of the lognormal fragility format that assumes that fragility curves are always monotonic functions of the ground acceleration. The large bias of the lognormal fragility curve from the zero-bias probability data point fragility curve is also visible for the 2 Hz equipment fragility curve at Node 576.

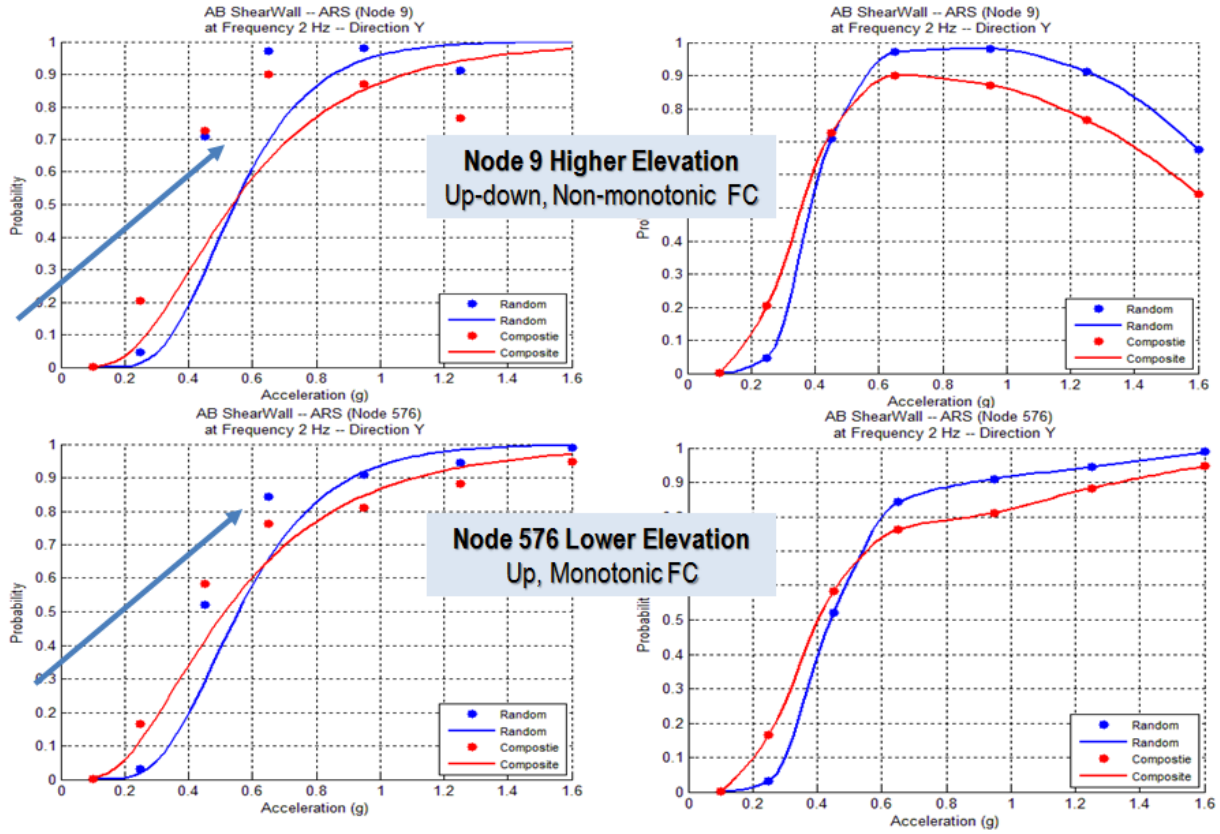

Figure 24 Fitted Lognormal (left) and Data-Point (right) Fragility Curves for 2Hz Frequency Equipment

Table 3 compares the overall predicted risks of the 2 Hz frequency equipment computed using the probability data-point fitted fragility curve versus the lognormal fitted fragility curve for few selected locations. The overall risks predicted by the traditional lognormal fragility curves are about 2-3 times smaller than the risks predicted by the zero-bias probability data-point fragility curves.

The Node 9 equipment risks are not included in Table 3 since the deviation of the fitted lognormal fragility curve from the computed probability data points is unacceptable large, as shown in Figure 23 upper plots.

Table 3 Overall Risks Computed for the Fitted Point-Data Curve vs. Fitted Lognormal Curve

	Point Data Curve Fitting			Lognormal Curve Fitting		
	Acceleration (g)			Acceleration (g)		
ISRS Node #	Random pf mean	2Hz pf C.O.V.		ISRS Node #	Random pf mean	2Hz pf C.O.V.
482	3.81E-005	0.53		482	1.57E-005	0.67
568	3.89E-005	0.57		568	1.46E-005	0.69
570	3.97E-005	0.59		570	1.44E-005	0.71
576	5.17E-005	0.79		576	1.24E-005	0.79

Based on the above results it appears that the traditional lognormal model for fragility curves is too crude or even inappropriate on a case-by-case basis. The breaking down of the traditional lognormal format is closely related to the highly nonlinear structure behaviour that produces a significant redistribution of the stiffness or stress/strain in the structure that affects both the structure and the equipment fragilities.

The nonlinear structure behaviour for large seismic inputs impacts most severely on on the ISRS shapes and amplitudes producing non-monotonic fragility curves for various frequency bands of potential interest. This could make the traditional lognormal format fragility model impractical is some situations as shown in Figure 23. For such situations different fragility curve models are more appropriate to be used in future.

The new ASCE 4-16 standard provides a robust physics-based probabilistic modelling for computing SSI response variations and fragility data that is a significant improvement over the simplistic traditional lognormal fragility model that is also based a lot on the "experts" subjectivity and uncapable to deal correctly with the real highly nonlinear structural behaviour for large seismic motions.

ASCE 4-16 Standard-Based Probabilistic SSI Analysis vs. EPRI-Based Deterministic SSI Analysis

Herein is a comparison between the probabilistic SSI analysis results using the new ASCE 4-16 standard-based methodology and the traditional EPRI-based methodology as applied in a number of seismic fragility analyses performed in US. The comparative analyses are performed for a single review level of 1.0g maximum ground acceleration that corresponds to the 1.e-5 annual occurrence probability GRS.

The investigated nuclear building is the same building shown in Figure 15. The nonlinear structure behaviour is based on the same modelling including the same BBCs and the Cheng-Mertz hysteretic model. However, the site-specific condition is quite different since it corresponds to a deep soft soil deposit.

Figure 25 shows the 60 probabilistic simulations of the horizontal and vertical GRS inputs at the ground surface based on the ASCE 4-16 Section 5.5 Method 2 that considers explicitly the spectral shape random variations. The GRS probabilistic model (ProEQUAKE module) was based a complete probabilistic site response analysis with the 1.e-5 UHRS input defined at the bedrock (Vs > 9,200 fps). Nonlinear hysteretic soil behaviour was included. The target and the simulated statistical GRS curves show a good matching.

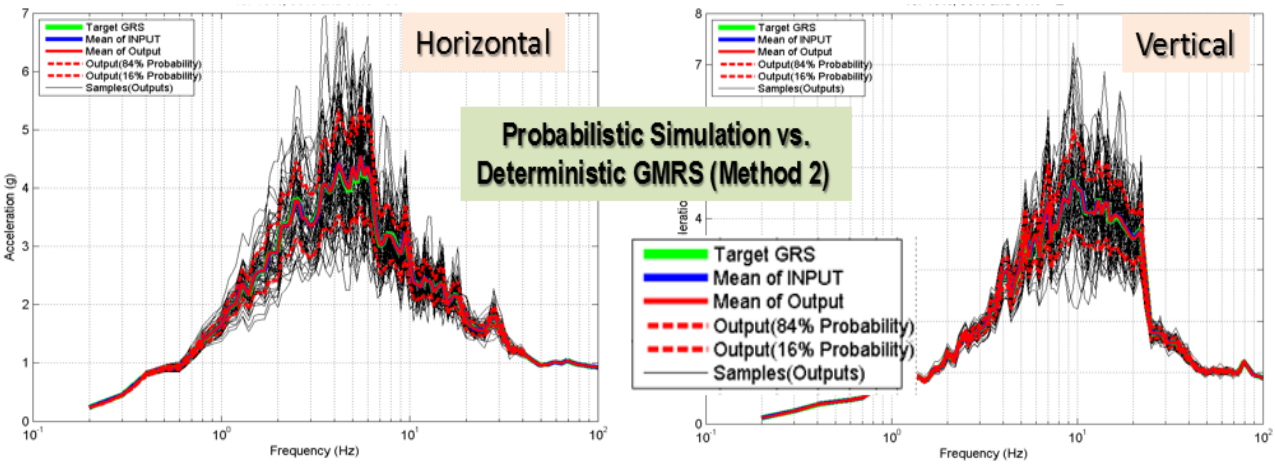

Figure 25 Simulated Probabilistic GRS Inputs for Horizontal and Vertical Directions

Figure 26 shows the 60 probabilistic simulations of the Vs soil profiles (black line) at the low shear strain level (ProSITE module). The target statistical Vs soil profiles (green) and the simulated statistical Vs profiles show a good matching. The 60 low-strain soil profile simulations were used for performing the

nonlinear site response analysis using the SHAKE methodology (SOIL module). The probabilistic soil material curves were simulated (ProSOIL module).

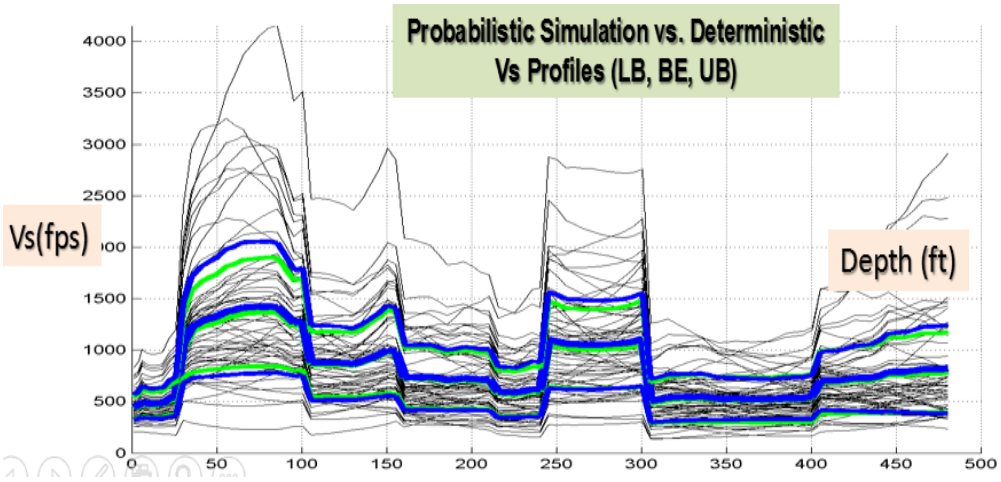

Figure 26 Simulated Probabilistic Vs Soil Profiles (shown down to the 500 ft depth)

The three deterministic soil profiles used in EPRI methodology, the lower-bound (LB) soil, the best-estimate (BE) soil, and the upper-bound (UB) soil were determined from the 60 simulated soil profiles which were computed for the effective shear strain in soil layers based on nonlinear. The LB, BE and UB soils corresponded to the 16% NEP, mean and 84% NEP statistical soil property values.

In the EPRI-based methodology, the "probabilistic" SSI analysis is performed for only five deterministic SSI analysis cases based on a center-composite experimental design scheme including 1) Best-estimate Structure and Best-estimate Soil (BEStr-BESoi), 2) Best-estimate Structure and Lower-bound Soil (BEStr-LBSoi), 3) Best-estimate Structure and Upper-bound Soil (BEStr-UBSoi), 4) Lower-bound Structure and Best-estimate (LBStr-BESoi), and 5) Upper-bound Structure and Best-estimate Soil (UBStr-BESoi).

The mean GRS or the GMRS input is considered for the seismic input in the EPRI-based methodology. For each SSI analysis case out of the five cases, the seismic input variability was considered by five sets of spectrum compatible acceleration histories based on "seed" records selected for similar sites.

The maximum SSI responses are computed for fifteen Soil variation cases (5 sets of acceleration inputs for each of the 3 soil variation cases, LB, BE and UB soils) and fifteen Structure variation cases (5 sets of acceleration inputs for each of the 3 structure stiffness variation cases). The structure stiffness variation cases include a linear elastic structure assumed to be fully cracked concrete everywhere that implies a 50% reduction of the uncracked stiffness with a coefficient of variation of 33%, i.e. the LB, BE and UB stiffness variations correspond to the cracked concrete stiffness times 0.67, (median) cracked stiffness, and cracked stiffness times 1.33. Concrete material damping was assumed to be 7% for all SSI analysis cases. In the EPRI methodology, the SSI response median and variations are computed considering all the seismic inputs, soil and structure variability cases. The total variation is computed based on the statistical variations computed separately for the seismic, soil and structure stiffness variations.

Figure 27 upper plot shows the computed statistical story drifts, namely, the probabilistic mean and 84% NEP values, using the ASCE 4-16 standard-based 60 probabilistic SSI simulations and the EPRI-based 25 deterministic simulation cases (5 cases are common), for the most affected shearwall panels in the structure. It should be noted that the ASCE 4-based probabilistic SSI vs. EPRI-based deterministic SSI

results are quite similar for some walls, as Panels 17, 19, 24 and 25, and quite different for other walls, as Panels 28 and 29, for which the EPRI results show very low SSI responses. The ASCE 4 based probabilistic simulation results shows that the critical wall panels are the Panels 28, 29, 15 and 16, while the EPRI based deterministic simulation results shows that the critical wall panels are the Panels 17, 24 and 25. These shown differences and trends are mainly due to the nonlinear behavior of the structure that produces much larger seismic response variations for the probabilistic simulations.

Figure 27 lower plot shows selected probabilistic wall hysteretic loop simulations (no. 10, 20, 30, 40, 50 and 60) for the transverse Panel 17 and the longitudinal Panel 28 near the building corner (see Figure 15 for the panel locations). It should be noted that the probabilistically simulated hysteretic responses are very different for the Panels 17 and 28 with different locations and orientations. The story drift variations are much more reduced for the Panel 17 than Panel 28. The Panel 28 story drift responses are highly scattered being dominated by two probabilistic simulations (no. 10 and 50) for which the SSI responses are few times larger than for the other simulations.

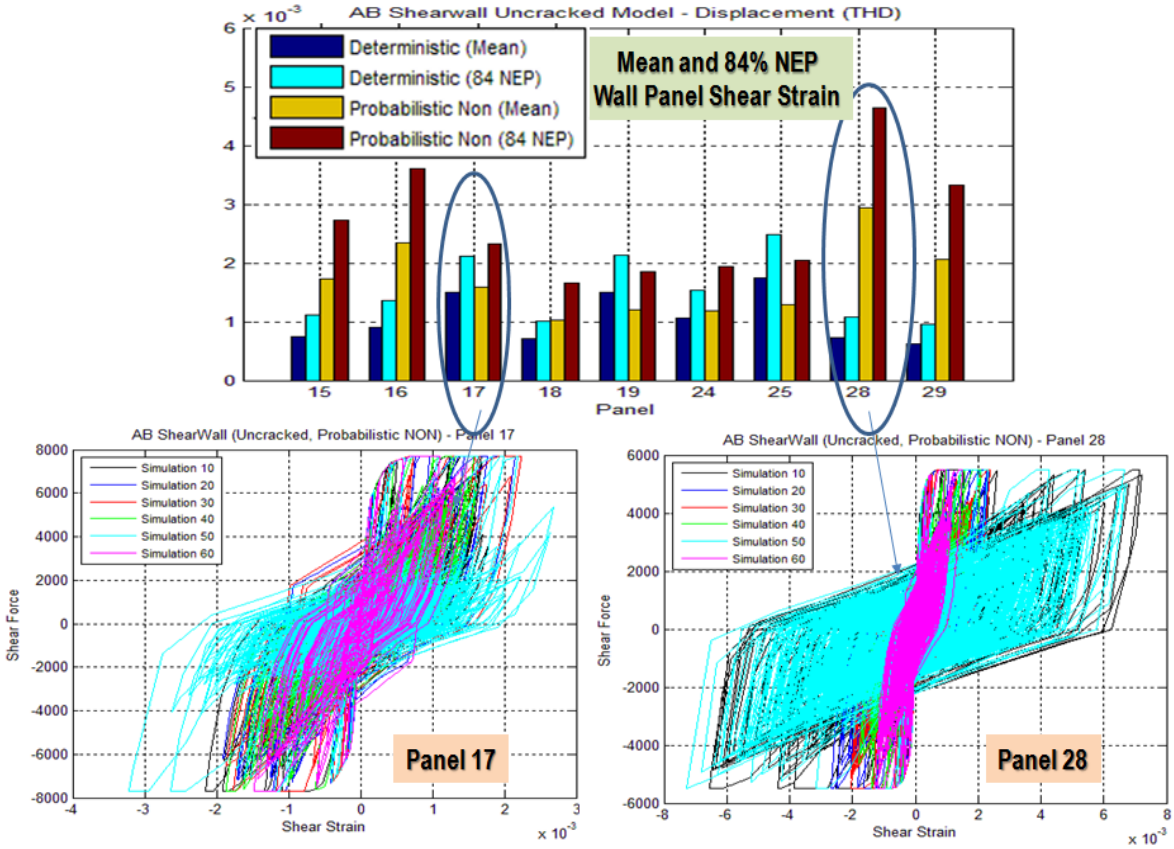

Figure 27 Predicted Statistical Shear Strain (upper plot) and Hysteretic Loops (lower plot) in Wall Panels

Figure 28 shows that the effects of the nonlinear structure behaviour are very significant for the severe seismic input of 1.0g ground acceleration. The nonlinear structure behaviour was included only in the ASCE 4-based probabilistic methodology, but not in the EPRI-based simplified methodology based on very limited deterministic SSI simulation cases.

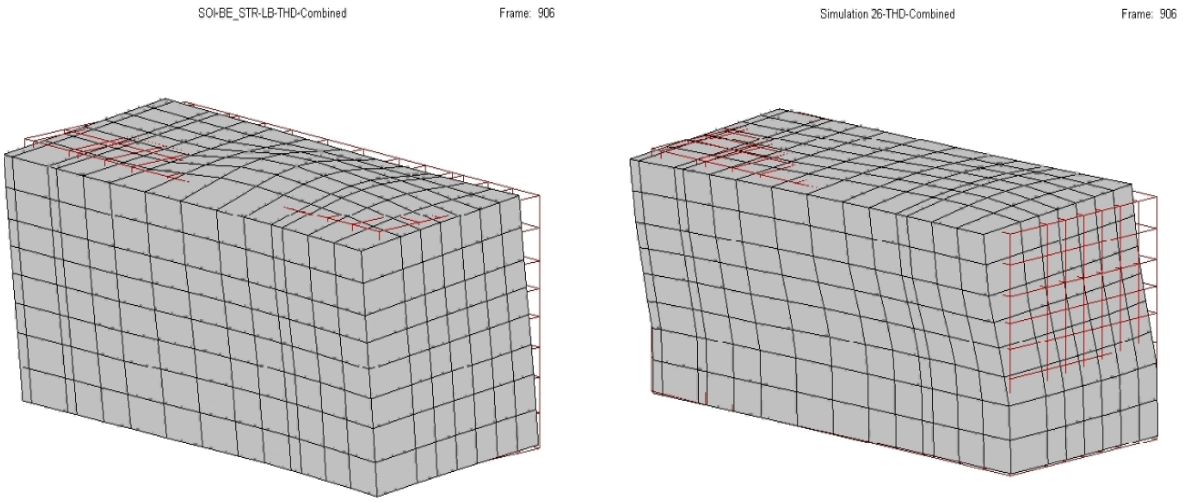

Figure 28 Effect of Nonlinear Behavior; EPRI Linear SSI (left) and ASCE 4 Nonlinear SSI (right)

Figures 29 and 30 show the computed ASCE 4-based probabilistic ISRS (60 simulations, mean and 84% NEP values) and EPRI-based deterministic ISRS (mean of 5 input sets for the 5 SSI analysis cases).

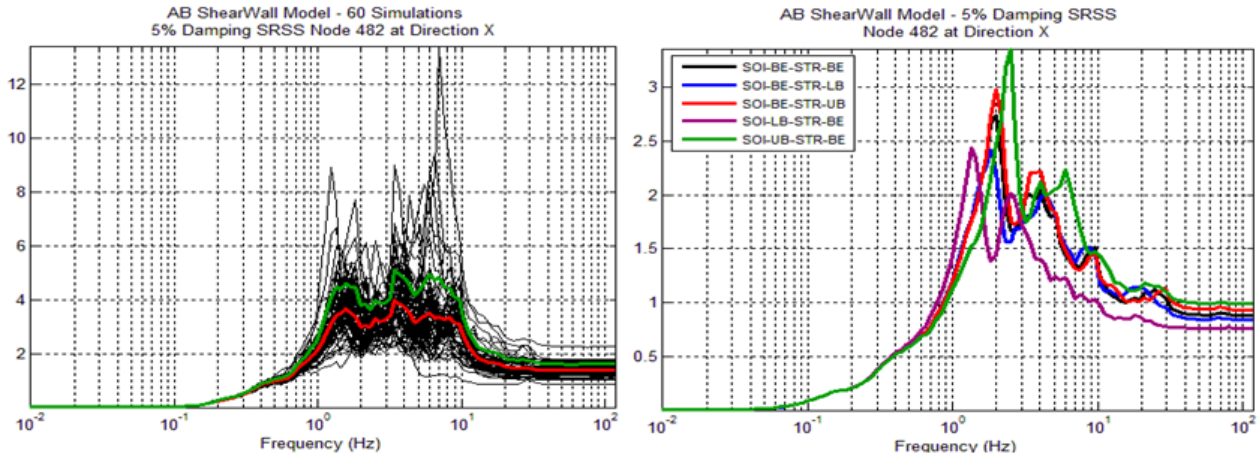

Figure 29 Comparative ASCE 4 Probabilistic (left) vs. EPRI Deterministic (right) ISRS at Node 482 (Basemat) in X-Direction

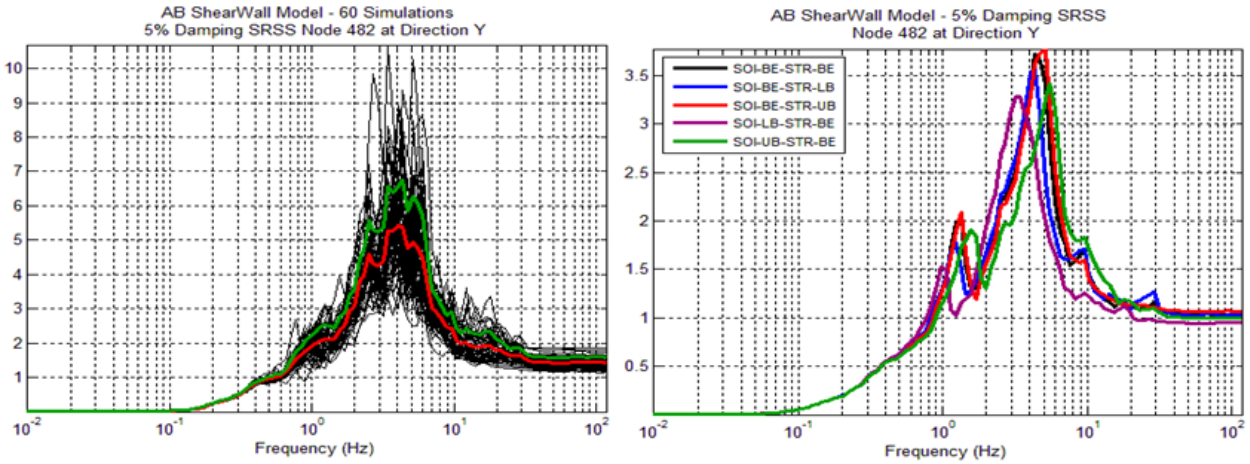

Figure 30 Comparative ASCE 4 Probabilistic (left) vs. EPRI Deterministic (right) ISRS at Node 482 (Basemat) in Y-Direction

The Figure 29 and 30 ISRS results for Node 482 at the basemat level indicate a significantly larger response variation for the ASCE 4 probabilistic SSI simulations than the EPRI deterministic SSI simulations. The implication of these different ISRS simulation results on the equipment risks or fragilities is shown in Table 4. The ASCE 4 based ISRS results produce 2 Hz frequency equipment risks that are up to two orders of magnitude larger than the EPRI based ISRS results for both X and Y directions.

The same conclusion is valid for the 8 Hz equipment risks at same Node 482 location, or for other locations as indicated by the computed risk results shown in Table 4. It should be noted that occasionally, the EPRI methodology provides conservative, or overly conservative risk results, as shown for the 2 Hz equipment fragility at Node 9 location in Y direction.

Table 4 Computed 2 Hz and 8 Hz Equipment Risks in X and Y Directions for Different ISRS Locations

ISRS X-Dir Prob Failure Vector

Frequency	2Hz		8Hz	
Node #	EPRI	ASCE	EPRI	ASCE
9	4.569765e-005	3.777722e-003	2.483734e-004	4.792264e-003
33	4.275362e-005	2.002747e-003	3.487098e-004	3.180917e-003
143	4.866542e-005	6.688034e-003	5.350239e-004	8.567610e-003
482	7.994426e-005	4.961024e-003	6.513999e-005	4.437899e-002
568	5.733355e-005	3.313409e-003	4.931325e-004	1.797246e-003
570	4.864856e-005	1.933949e-003	1.929920e-004	1.886620e-002
576	5.392025e-005	3.222089e-003	3.879110e-004	1.957318e-002

ISRS Y-Dir Prob Failure Vector

Frequency	2Hz		8Hz	
Node #	EPRI	ASCE	EPRI	ASCE
9	2.317968e-002	1.755416e-004	1.005848e-003	2.620980e-005
33	1.733793e-002	1.140928e-004	1.055803e-004	2.442733e-003
143	2.115206e-002	1.367721e-004	4.619638e-004	1.109834e-003
482	5.026507e-004	9.617958e-002	7.939274e-005	4.233506e-002
568	4.309107e-003	5.703761e-005	2.649222e-003	2.534387e-002
570	1.041260e-002	6.178707e-006	1.584783e-003	6.712163e-003
576	1.905288e-002	3.277204e-006	9.061175e-004	1.206431e-002

The above results show that the SSI structural behaviour is very different for the ASCE 4 probabilistic nonlinear SSI simulations (nonlinear structure model) and the EPRI deterministic linear SSI simulations (linear cracked structure model with a 0.5 mean/median stiffness reduction and 7% damping).

The ASCE 4 probabilistic SSI modelling including the nonlinear structure behaviour captures well the physical-behaviour of the concrete structure. The ASCE 4 probabilistic-based fragility results are quite different than the EPRI deterministic-based fragility results. Differences in the predicted risks/fragilities could be up to two-three orders of magnitude.

CONCLUSIONS

The paper illustrates the application of the probabilistic seismic SSI analysis to the nuclear structures based on the new ASCE 04-16 standard recommendations applicable to both the design-basis level (DBE) applications and the beyond design-basis level (BDBE) applications including fragility analyses.

For the DBE applications, significant differences were noted between the probabilistic SSI and deterministic SSI responses for the deeply embedded SMR structure. There is a need for having a larger number of rigorous comparative probabilistic-deterministic investigations based on the ASCE 4-16

standard recommendations for both shallow and deeply embedded structures modeled using detailed FE models with elastic foundations (not just sticks with rigid basemats).

The ASCE 4 probabilistic SSI modelling including the nonlinear structure behaviour captures well the physical-behaviour of the concrete structures for the BDBE applications. The new ASCE 4-16 standard provides a robust physics-based probabilistic modelling for computing the SSI response variations as a basis for predicting the seismic fragilities of the SSCs for the new design nuclear plants. The ASCE 4-16 standard probabilistic-based SSI methodology provides a major improvement over the more simplistic traditional EPRI deterministic-based SSI methodology that was applied over the last three decades for performing fragility analyses for the existing nuclear plants in operation.

REFERENCES

American Society of Civil Engineers (2017), ASCE 4-16 Standard for "Seismic Analysis for Safety-Related Nuclear Structures and Commentary, April

Gergely, P.(1984)."Seismic Fragility of Reinforced Concrete Structures and Components for Application in Nuclear Facilities", Prepared for USNRC, Published as NUREG/CR-4123

Ghiocel, D.M (2016). "New ASCE 4-Based Probabilistic Nonlinear SSI Analysis for Improving Seismic Fragility Computations", Session VIII–Uncertainty in Soil-Structure Interaction (SSI) Analysis, Invited Panelist,10th Nuclear Plants Current Issues Symposium: Assuring Safety against Natural Hazards through Innovation & Cost Control, Charlotte, North Carolina, December 11-14.

Ghiocel, D.M. (2016). "Probabilistic SSI Analysis Per ASCE 4-16 Standard; A Significant Improvement for Seismic Design-Basis Analysis and Fragility Calculations", US DOE Natural Phenomena Hazards Meeting Germantown, MD, October 18-19

Ghiocel Predictive Technologies, Inc. (2016). "ACS SASSI - An Advanced Computational Software for 3D Dynamic Analyses Including SSI Effects", ACS SASSI Version 3.0 User Manuals, December

Ghiocel, D.M., (2015). "Fast Nonlinear Seismic SSI Analysis Using A Hybrid Time-Complex Frequency Approach for Low-Rise Nuclear Concrete Shearwall Buildings", the SMiRT23 Conference for NPP Structures, August 10-14

Ghiocel, D.M., "Probabilistic-Deterministic SSI Studies for Surface and Embedded Nuclear Structures on Soil and Rock Sites", the SMiRT23 Conference for NPP Structures, August 10-14

Ghiocel, D.M., (2014)."Comparative Probabilistic-Deterministic and RVT-based SASSI Analyses of Nuclear Structures for Soil and Rock Sites", 2-Day U.S. Department of Energy Natural Phenomena Hazards Meeting, Germantown, MD, USA, October 21-22

Gulec, C.K. and A.S. Whittaker (2009). "Performance-Based Assessment and Design of Squat Reinforced Concrete Shear Walls", Technical Report, MCEER, No. 09-0010, Sept. 2009.

Reed J.W. and Kennedy R.P (1994), "Methodology for Developing Seismic Fragilities", EPRI, EPRI TR# 103959

Wood, S., "Shear Strength of Low-Rise Reinforced Concrete Walls," ACI Structural Journal, Vol. 87, No. 12, pp. 99-107, 1990.